Case Studies in Thermal Engineering 12 (2018) 833–842

Contents lists available at ScienceDirect

Case Studies in Thermal Engineering

journal homepage: www.elsevier.com/locate/csite

Cooling performance of Al_2O_3-water nanofluid flow in a minichannel with thermal buoyancy and wall conduction effects

C.J. Ho[a,*], Yu-Hui Chiou[a], Wei-Mon Yan[b,c,**], Mohammad Ghalambaz[d]

[a] Department of Mechanical Engineering, National Cheng-Kung University, Tainan 70101, Taiwan
[b] Department of Energy and Refrigerating Air-Conditioning Engineering, National Taipei University of Technology, Taipei 10608, Taiwan
[c] Research Center of Energy Conservation for New Generation of Residential, Commercial, and Industrial Sectors, National Taipei University of Technology, Taipei 10608, Taiwan
[d] Department of Mechanical Engineering, Dezful Branch, Islamic Azad University, Dezful, Iran

ARTICLE INFO

Keywords:
Al_2O_3-water nanofluid
Mixed convection
Thermal buoyancy effect
Wall conduction effect
Minichannel

ABSTRACT

The effect of highly conductive thick walls on the mini channel heat transfer performance is systematically addressed while two constant heat flux sources are considered at the bottom of the channel. The influence of using different mass fractions of Al_2O_3 nanoparticles dispersed in water as working fluid are studied. The buoyancy effects on the thermal performance and pressure drop of the mini channel are also investigated. The finite volume method is employed to simulate the flow and heat transfer of nanofluid in the channel. The results show that the axial heat transfer is an important effect in mini channels with thermal conductive walls and should be taken into account. It is found that the presence of nanoparticles with the mass fraction of 5% and 10% drops the maximum temperature (and increases the pressure drop) by 1.28% (17.0%) and 1.48% (41.0%), respectively when Reynolds number is 500 and neglecting buoyancy effects. The presence of buoyancy effects reduces the pressure drop by 21.08% in a case with Reynolds number 500 and the nanoparticles mass fraction 5%. This is while the presence of buoyancy effects would decrease the maximum temperature by 1 °C.

1. Introduction

The advancement of industrial technology has decreased the size of electronic components by utilizing advance packaging systems. The miniaturization of electronic components has increases the power generation in these component. Reduction in size and augmentation in heat generation has drastically increased the surface heat flux per unit of area. This increasingly high power density heat flux demands efficient and powerful cooling systems [1,2]. Thus, advancing cooling technology of the electronic components is a primary key issue in development and further miniaturization of these components. The increase of cooling power can be handled by the increase of the heat transfer rate and improvement of the heat dissipation mechanisms.

The millimeter size micro-channel heat sink is one of the heat exchangers with the advantages of high heat capacity and the ability to remove a large amount of heat from a small volume by benefiting a large heat exchange area. Micro-channel is capable of meeting the cooling power requirements of today's electronic components with high heat flux. The heat exchange area can be further

* Corresponding author.
** Corresponding author at: Department of Energy and Refrigerating Air-Conditioning Engineering, National Taipei University of Technology, Taipei 10608, Taiwan.
E-mail addresses: cjho@mail.ncku.edu.tw (C.J. Ho), wmyan@ntut.edu.tw (W.-M. Yan).

https://doi.org/10.1016/j.csite.2018.11.002
Received 27 September 2018; Accepted 4 November 2018
Available online 12 November 2018
2214-157X/ © 2018 The Author. Published by Elsevier Ltd. This is an open access article under the CC BY-NC-ND license (http://creativecommons.org/licenses/BY-NC-ND/4.0/).

Nomenclature

A^+	Area (m^2)
$AR_{bw,x}$	Aspect ratio of the bottom wall
$AR_{ch,x}$	Aspect ratio of the channel wall
$AR_{cw,x}$	Aspect ratio of the top wall
$\dot{Q}$	Flow rate (m^3/s)
Δp	Pressure drop (Pa)
$\Delta Tref,bf$	Reference temperature difference
cp	Specific heat at constant pressure
$d+$	Average particle size
$D+h$	Hydraulic diameter
g	Gravitational constant
Gr	Grashof number
H	Dimensionless height
h	Heat transfer coefficient (W/m·K)
k	Conductive thermal *coefficient* (W/m^2·K)
L^+	The channel length
Nu	Nusselt number
n	Surface normal vector
p	Pressure (kPa)
Pe	Peclet number
Pr	Prandtl number
q	Heat transfer (W)
q''	Heat flux (W/m^2)
R	Thermal resistance
Ra^*	Rayleigh number
Re	Reynolds number
Ri^*	Richardson number
T	Temperature (°C)
u^+	Fluid velocity
$\boldsymbol{V}$	Velocity vector
W	Dimensionless width

Greek symbol

α	Thermal diffusivity (m^2/s)
β	Coefficient of thermal expansion (1/K)
ε	Ratio of comparison
θ	Dimensionless temperature
μ	Dynamic viscosity ($N{\cdot}s/m^2$)
ρ	Density (kg/m^3)
ϕ	Nanoparticles volume fraction
ω	Mass fraction of nanoparticles

Subscript symbol

b	Bulk (average) properties
bf	Base fluid
bf/nf	Base fluid to nanofluid ratio
bw	Bottom wall solid
ch	Channel
ch,b	The interface between the flow in channel and bottom wall
ch,s	The interface between the flow in channel and side wall
ch,t	The interface between the flow in channel and top wall
$cond$	Conduction
cw	Top wall
d	Outlet adiabatic section
$h1$	First heating section
$h2$	Second heating section
i	Inner wall
in	Inlet
int	Internal
max	Maximum
nf	Nanofluid
np	Nanoparticle
o	Outer wall
sw	Side wall
u	Inlet adiabatic section
w	Wall surface
x, y, z	x, y, and z directions

Super scripts

*	Ratio
+	Dimensional parameter

increased by increasing the number of fins in the heat sink, but it may be at the expense of pressure drop, so a balance between heat transfer efficiency and pressure drop is required. Millimeter micro-channel heat sink and nanofluid have been put into research by many scholars, and it has been proved that it can effectively improve the heat transfer rate and improve the cooling power efficiency.

The micro-channel heat sink system was first proposed by Tuckerman and Pease [3]. The proposed micro channel was a rectangular duct made of silicon. The experimental results of Tuckerman and Pease demonstrate that a micro channel with working fluid of water is capable of removing 790 W/cm^2 with the temperature difference of 71 °C. This is an ultra-high heat capacity removal for a compact heat exchanger. Qu and Mudawar [4] used pure water as the working fluid in the rectangular micro-channel to compare the experimental and numerical simulations, and verified that the traditional equation can be applied to the micrometer flow channel. Lee et al. [5] studied the heat transfer phenomenon of rectangular flow channels, and proposed that the heat transfer effect is better when the flow channel size is smaller and the aspect ratio is larger. They verified their experimental results by numerical methods. Le and Garimella [6] demonstrated that the flow channel has a relationship between its aspect ratio and Nusselt number, and proposes an accurate prediction formula for Nusselt number as a function of channel aspect ratio.

Under the development of nanotechnology, in 1995, Choi [7] proposed the term nanofluid to add nanometer-sized solid particles to water to form nanofluids. A nanofluid is a stable mixture of nanoparticle and a traditional working fluid. The addition of nanoparticles to working fluids can effectively improve the overall physical properties of the working fluid, and hence, the nanofluids can be proposed as an alternative to traditional working fluids [8,9]. Although most of the conventional cooling systems employ the traditional working fluids (water or air) to transfer energy by sensible heat change, in recent years, many researchers have proposed to replace the working fluid with nanofluid. There are excellent comprehensive reviews on the application and thermo physical behaviour of nanofluids including the study of Saidur et al. [8], Khanafer and Vafai [9,10], Mahian et al. [11], and Devendiran and

Amirtham [12]. The literature review shows that there are some analytical models for evaluating the thermophysical properties of nanofluids. Two of the well-known models for the thermal conductivity evaluation of nanofluids are the Maxwell and Hamilton and Crosser models. The well-known model for dynamic viscosity of nanofluids is the Brinkman model.

Zaraki et al. [13] have studied the effect of size, shape, and type of nanoparticles in nanofluids and proposed a linear model for the thermal conductivity and dynamic viscosity behaviour of nanofluids. They introduced two non-dimensional parameters of number of thermal conductivity (Nc) and number of dynamic viscosity (Nv) for nanofluids. Khanafer and Vafai [9] have reviewed the thermophysical properties of nanofluids and concluded that the well-known Maxwell and Hamilton and Crosser and the Brink man model are not capable of predicting the thermo physical properties of nanofluids due to the fact that these models are independent of the nanoparticle size. Hence, by taking into account the size and temperature of the nanofluid, they have proposed some mathematical relations based on the extensive analysis of available experimental data.

In the recent years, various aspects of heat transfer in micro-channels have been addressed experimentally and numerically. Lee and Mudawar [14] experimentally investigated the influence of addition of alumina nanoparticles to the water on the heating behaviour of a micro-channel. The results show that the heat transfer efficiency can be effectively improved. Chuan et al. [15] have proposed a new design concept for micro-channels by replacing the heat sink fins with a thermal conductive porous media. The results show that the drag reduction efficiency intensely depends on the porous medium characteristics. They reported that the pressure drop can be reduced by using a porous medium with high permeability. Leng et al. [16] have studied cooling performance of micro-channels using CO_2 as coolant. The results show that a micro channel working with CO_2 requires larger number of channels compared to a micro-channel which works with water as coolant.

Mahian et al. [17] have investigated the enhancement of using nanofluids in mini-channels for solar collector applications. They have studied four different nanofluids in water including Cu, Al_2O_3, TiO_2, and SiO_2. It is found that Al_2O_3/water nanofluids provides the highest heat transfer coefficient in the tubes under the turbulence flow. Ho et al. experimentally and numerically [18] have addressed the forced convection of alumina nanofluid in a circular tube. It is found that the increase of the working temperature of nanofluid increases the effectiveness of using nanoparticles. In another study, Ho et al. have studied the cooling performance of using microencapsulated phase change material (MEPCM) suspensions with water in mini-channel heat sinks with a uniform rectangular cross section [19], parallel and divergent mini-channel heat sinks [1,2]. They studied different divergent angles and various volume fractions of additives under different heat fluxes. The results show that diverging the mini-channels boosts the influence of the presence of microencapsulated material (MEPCM) in heat sinks. Ghani et al. [20] have performed an excellence review on the hydrothermal performance of micro-channel heat sinks.

The literature review shows that the buoyancy effects and the systematic analysis of the influence of the channel walls on the heat transfer performance of mini channels for nanofluids has not been investigated yet. The present study aims to analysis the effect of the presence of alumina nanoparticles in water as the working fluid in a mini channel with thick highly conductive walls. The contribution of the buoyancy effects on the thermal performance and pressure drop in the mini-channel is also addressed.

2. Problem description and mathematical model

Fig. 1 shows the schematic view of the physical model of the rectangular millimeter channel with thick walls. The three dimensional model of the mini-channel is consist of a channel with a thick solid wall in which its top and side walls are well insulated while two small areas of its bottom are subject to a constant heat flux of q''_h. The inlet (L_u^+) and outlet (L_d^+) region of the channel are well insulated which are considered as adiabatic with zero heat flux. Fig. 1(a) and (b) illustrate the side cross sectional and the cross

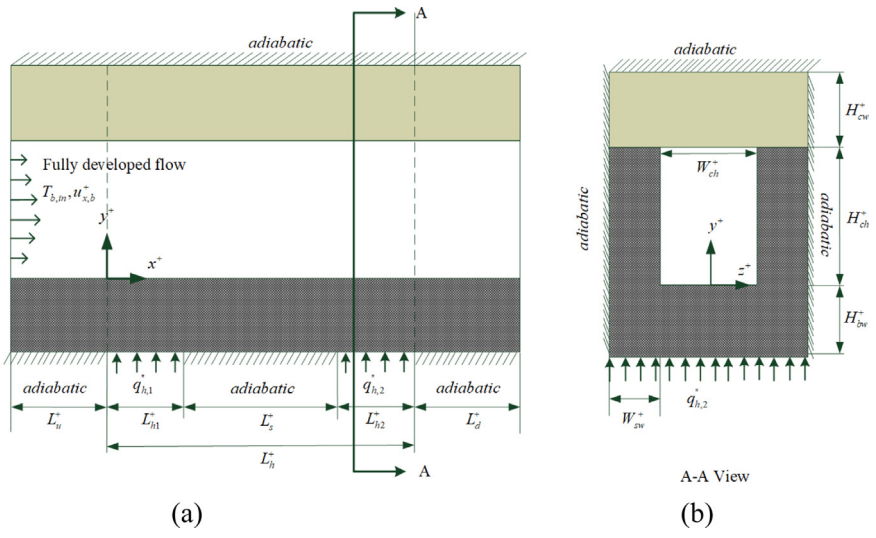

Fig. 1. The schematic view of the physical model of rectangular mini-channel; (a): the side view, (b):.

sectional view of the physical model of the channel, respectively. As seen in Fig. 1(a), there are two separate sections inside the channel which are subject to the uniform heat fluxes of $q''_{h,1}$ and $q''_{h,2}$. The heat fluxes induce a temperature gradient in the solid wall of the channel and increases the temperature of the channel walls. A nanofluid with the uniform temperature of $T_{b,in}$ and fully develop velocity of $u^{+}_{x,b}$ enters the channel and flows in the adiabatic entry region. The nanofluid then passes over the heated sections of the channel and absorbs the heat from the channel walls by convection. After that, the nanofluid reaches to the outlet region and flows out of the channel through the outlet section. The geometrical details of the mini-channel model and the utilized coordinate system are indicated in Fig. 1. The top thick wall of the channel is made of acrylic (PMMA) while the bottom and side walls of the channel, the black blocks in the schematic model, are made of copper with high thermal conductivity. The working fluid which passes through the channel contains very fine alumina nanoparticles of size 22.2~47.7 nm which are well dispersed in the base fluid of water. The nanoparticles are spherical shape which the state of their crystal structure is γ. The density and specific thermal capacity of the nanoparticles are $\rho_{nf} = 3600\,\mathrm{kg/m^3}$ and $c_{p,np} = 765\,\mathrm{J/kg\,K}$, respectively.

To model the mixed convection heat transfer of the nanofluid inside the channel, the following assumptions are considered: The nanofluid is a homogeneous mixture of nanoparticles and the base fluid, and there is no chemical change between the particle and the fluid interface. The particles are rigid and uniform spheres that are in local thermal equilibrium with the base fluid. The nanofluid is an incompressible Newtonian fluid, and the flow in the channel is steady-state and laminar. The temperature changes are limited, and Boussinesq approximation is applicable. Hence, the thermophysical properties of the nanofluid and solid materials are constant. The buoyancy effects due to the density change are modeled using the Boussinesq model. The radiation effects and viscous dissipation effects are negligible. The channel is symmetric in half side section at the plane of z = 0 parallel to x-y plane. Hence, in order to reduce the computational costs, the symmetric model is utilized. Considering these assumptions, the governing equations of the nanofluid flow and heat transfer can be represent in dimensionless forms:

Continuity equation

$$\frac{\partial u_x}{\partial x} + \frac{\partial u_y}{\partial y} + \frac{\partial u_z}{\partial z} = 0 \tag{1}$$

Momentum equations

$$u_x\frac{\partial u_x}{\partial x} + u_y\frac{\partial u_x}{\partial y} + u_z\frac{\partial u_x}{\partial z} = -\frac{\partial p}{\partial x} + \frac{D_h}{\mathrm{Re}_{bf}}\nu^*_{m/bf}\left(\frac{\partial^2 u_x}{\partial x^2} + \frac{\partial^2 u_x}{\partial y^2} + \frac{\partial^2 u_x}{\partial z^2}\right) \tag{2a}$$

$$u_x\frac{\partial u_y}{\partial x} + u_y\frac{\partial u_y}{\partial y} + u_z\frac{\partial u_y}{\partial z} = -\frac{\partial p^+}{\partial y^+} + \frac{D_h}{\mathrm{Re}_{bf}}\nu^*_{m/bf}\left(\frac{\partial^2 u_y}{\partial x^2} + \frac{\partial^2 u_y}{\partial y^2} + \frac{\partial^2 u_y}{\partial z^2}\right) + \frac{Ri^*_{T,bf}}{D_h}\beta^*_{T,m/bf}\theta g \tag{3b}$$

$$u_x\frac{\partial u_z}{\partial x} + u_y\frac{\partial u_z}{\partial y} + u_z\frac{\partial u_z}{\partial z} = -\frac{\partial p}{\partial z} + \frac{D_h}{\mathrm{Re}_{bf}}\nu^*_{m/bf}\left(\frac{\partial^2 u_z}{\partial x^2} + \frac{\partial^2 u_z}{\partial y^2} + \frac{\partial^2 u_z}{\partial z^2}\right) \tag{2c}$$

Energy equation of nanofluid

$$\frac{D_h}{\mathrm{Re}_{bf}\mathrm{Pr}_{bf}}\frac{\partial\theta}{\partial Fo} + u_x\frac{\partial\theta}{\partial x} + u_y\frac{\partial\theta}{\partial y} + u_z\frac{\partial\theta}{\partial z} = \alpha^*_{m/bf}\frac{D_h}{\mathrm{Re}_{bf}\mathrm{Pr}_{bf}}\left(\frac{\partial^2\theta}{\partial x^2} + \frac{\partial^2\theta}{\partial y^2} + \frac{\partial^2\theta}{\partial z^2}\right) \tag{3}$$

Energy equation of solid wall

$$\alpha^*_{cw/bf}\left(\frac{\partial^2\theta}{\partial x^2} + \frac{\partial^2\theta}{\partial y^2} + \frac{\partial^2\theta}{\partial z^2}\right) = 0 \tag{4}$$

In the above non-dimensional equations, *Pr* is the Prandtl number, *Ra* is the Rayleigh number, *Gr* is the Grashof number, *Ri* is the Richardson number, *Re* is the Reynolds number, *Pe* is the Peclet number which are defined as:

$$Ra^*_{T,bf} = \frac{g\beta_{T,bf}\Delta T_{ref,bf}W^{+3}_{ch}}{\alpha_{bf}\nu_{bf}},\ Gr^*_{T,bf} = \frac{Ra^*_{T,bf}}{\mathrm{Pr}_{bf}} = \frac{g\beta_{T,bf}\Delta T_{ref,bf}W^{+3}_{ch}}{\nu^2_{bf}},$$
$$Ri^*_{T,bf} = \frac{Gr^*_{T,bf}}{\mathrm{Re}^2_{bf}},\ \mathrm{Re}_{bf} = \frac{u^+_{x,fd,b}D^+_h}{\nu_{bf}},\ \mathrm{Pr}_{bf} = \frac{c_{p,bf}\nu_{bf}\rho_{bf}}{k_{bf}},\ Pe_{bf} = \frac{u^+_{x,fd,b}D^+_h}{\alpha_{bf}} \tag{5}$$

The corresponding non-dimensional boundary equations are:

At inlet: $u = u_{d,nf}/u_{x,b}$ and $\theta = \theta_{in}$ (6a)

At outlet: $\frac{\partial\theta}{\partial x} = 0$ and $\mathrm{p} = \mathrm{po}/\rho_{bf}u^{+2}_{b,in}$ (6b)

At interface of the walls and nanofluid: $\mathbf{V} = 0$ and $k^*_{nf/bf}\left.\frac{\partial T}{\partial n^+}\right|_{nf} = k^*_{cw/bf}\left.\frac{\partial T}{\partial n^+}\right|_{cw}$ and $\theta_{nf} = \theta_{cw}$ (6c)

At adiabatic surfaces of channel: $\frac{\partial \theta}{\partial n} = 0$ (6d)

At channel surface subject to heat flux: $\frac{\partial \theta}{\partial n} = -\frac{k^*_{nf/bf}}{k^*_{sw/bf}}$ (6e)

At the wall symmetry plane$(z = 0)\frac{\partial \theta}{\partial z} = 0,\ \frac{\partial u_x}{\partial z} = 0,\ \frac{\partial u_y}{\partial z} = 0,\ u_z = 0$ (6f)

The thermophysical properties of nanofluid are evaluated using the comprehensive review study of Khanafer and Vafai [9]. The important flow and heat transfer characteristics are defined as:

$$u^+_{b,x}(x^+) = \frac{1}{A^+_{ch,x}(=H^+_{ch}W^+_{ch})}\int_{y^+=0}^{H^+_{ch}}\int_{z^+=-W^+_{ch}/2}^{W^+_{ch}/2} u^+_x dy^+ dz^+ \tag{7a}$$

$$\mathbf{T}_{b,x} = \frac{1}{\dot{Q}c_{p,m,0}}\int_{A^+_{ch,x}} c_{p,m}u^+_x T dA^+_{ch,x} \tag{7b}$$

$$\theta_{b,x} = \frac{T_b(x^+) - T_{b,in}}{\Delta T_{ref,bf}} \tag{7c}$$

$$\varepsilon_T = \frac{T_{b,nf} - T_{b,bf}}{T_{b,bf}} \tag{7d}$$

where $u^+_{b,x}$, $T_{b,x}$ and $\theta_{b,x}$ are the bulk velocity, bulk temperature and non-dimensional bulk temperature. Here, $\dot{Q}(=u^+_{x,b}A^+_{ch,x})$ is the channel flow rate. ε_T denotes the temperature ratio enhancement of using nanofluids compared to the base fluid, and subscript of b denotes the bulk temperature.

3. Numerical solution method

The Finite Volume Method (FVM) is employed to numerically integrate the differential Eqs. (1)–(4) with the corresponding boundary conditions Eq. (6). The convective term is processed by the quadratic upwind interpolation for convective kinematics. The solution area can be divided into a base/side wall solid zone, a channel fluid zone, and a roof solid zone. The three parts of the solution area are solved consequently from the inlet section and from bottom to top and in longitudinal direction to the outlet using the Line SOR longitudinal iteration method. At the interface between the solid zone and the fluid zone, the temperature continuity and heat flux continuity is monitored to be satisfied. The temperature is calculated from the solid zone to the boundary temperature of the fluid zone. The heat flux crossing the fluid zone is set equal to the heat flux crossing the solid zone. The velocity is iteratively calculated in a pseudo-transient mode. The convergence for the solution over the entire the physical zones is checked. If the convergence criterion is not satisfied, the iteration is performed again according to the above method.

In numerical simulation, the grid size is an important key parameter which affects the computational costs and the accuracy of the results. Hence, various grid sized are tested to study the influence of the grid size on the results. The grid sizes are reported for the total number of grids, the grids in the liquid zone, and the grids in the solid walls of the channel. Since the base solid region is a material with a large thermal conductivity (copper), the temperature gradient is small, so the required number of meshes is low. In contrast, the thermal conductivity of water or nanofluid as the working fluid in the fluid region of the channel is low, and the temperature gradient is large, so a dense grid is required to adequately capture the temperature gradients.

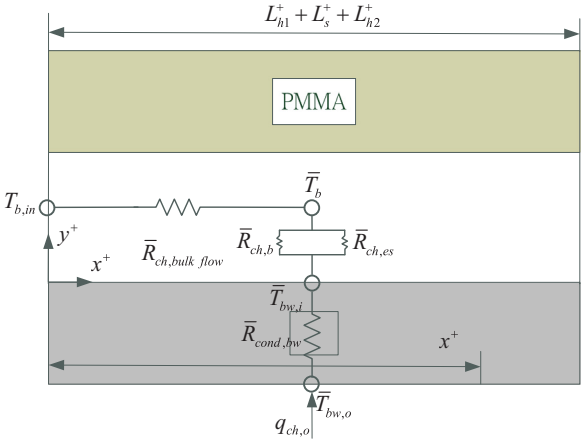

Fig. 2. Schematic view of the thermal resistance model in the channel with highly conductive thick walls.

4. Results and discussion

There are several conduction and convection mechanism between the heated zone and the working fluid affecting the thermal behaviour of the milometer channel with highly conductive thick walls. In order to understand the complexity of the heat transfer mechanisms, a resistance model of heat transfer in channel is depicted in Fig. 2. As seen in this figure, there is a heated zone subject to heat flux $q_{ch,o}$ at the bottom of the channel. This part of channel receives the heat flux and gets hot to the average temperature of $\bar{T}_{bw,o}$. There is a conduction thermal resistance between the hot temperature of $\bar{T}_{bw,o}$ and the inner surface of the channel walls with the average temperature of $\bar{T}_{bw,i}$. This resistance between $\bar{T}_{bw,o}$ and $\bar{T}_{bw,i}$ is denoted by $\bar{R}_{cond,bw}$. When the heat flux reaches to the channel wall through the resistance of $\bar{R}_{cond,bw}$, there are two convective heat transfer mechanisms between the channel surfaces ($\bar{T}_{bw,i}$) and the bulk temperature of the fluid ($\bar{T}_b$) inside the channel; one through the bottom of the channel wall with the thermal resistance of $\bar{R}_{ch,b}$ and the other is the convective heat flux through the other walls of the channel with the thermal resistance of $\bar{R}_{ch,es}$. In addition, there is an axial heat transfer toward the inlet region due to the conduction in the fluid between the fluid bulk temperature ($\bar{T}_b$) and the inlet temperature $T_{b,in}$ which occurs through the thermal resistance of $\bar{R}_{ch,bulk\,flow}$.

Table 1 shows the maximum temperature at the two heated zones, $T_{h,1,max}$ and $T_{h,2,max}$. The results of this table indicate that the increase of the mass fraction of nanoparticles decreases the maximum temperatures. When $\omega_{np} = 5\%$ and $Re_{bf} = 500$, the presence of alumina nanoparticles drops the maximum temperature of the first and second heated zones by 1.28% and 1.15% respectively. In the case of $\omega_{np} = 10\%$ and the same Reynolds number, the temperature drop over the first and second heated zones is 1.48% and 1.36% respectively. Table 2 shows the pressure drop in the channel. This table demonstrates that the increase of mass fraction of nanoparticles increases the pressure drop in the channel. The maximum pressure drops occur at $Re_{bf} = 2000$ with $\varepsilon_p = 20.3\%$ ($\omega_{np} = 5\%$) and 40.7% ($\omega_{np} = 10\%$).

Fig. 3 depicts the velocity contours and vectors at different cross sections of the channel. It can be seen from Fig. 3 that at the beginning of the heating section ($x_b = 0$), the secondary flows in the channel are small, and the velocity is mainly the flow direction (u_x^+) velocity component, and the lateral (u_z^+) and gravity direction (u_y^+) velocity components are negligible. After entering the heating section, the temperature gradient near the wall increases. Moving toward the heated zones, the velocity component of u_y^+ and u_z^+ get stronger next to the bottom and side wall of the channel where the temperature is high. The lateral flow induces a circulation shape counterclockwise rotation flow which begins from the bottom and side wall of the channel, which are hot, and moves toward the top wall of the channel, which is not as hot as the side wall and bottom wall. This circulation flow is due to the buoyancy effects. When the Reynolds number is low, the buoyancy effect is more obvious.

Table 3 shows the pressure drop due to the presence of the buoyancy effects for pure water ($\omega_{np} = 0\%$), nanofluid with mass fractions of $\omega_{np} = 5\%$ and $\omega_{np} = 10\%$. At low Reynolds number of 500, the presence of 5% and 10% mass fraction of nanoparticles increases the pressure drop by 16.8% and 40.3%, respectively. The comparison between the results of this table reveals that the presence of buoyancy effects decreases the pressure drop for both cases of the pure fluid and the nanofluid. Considering the relative pressure drop as ε = (Δp with buoyancy -Δp without buoyancy)/Δp without buoyancy, the relative pressure drop between the presence and absence of buoyancy effects is 21.08% for the case of nanofluid with 5% mass fraction of nanoparticles and Reynolds number of 500.

The non-dimensional bulk temperature for the fluid inside the channel ($\theta_{b,x}$) and the non-dimensional average temperature for the channel bottom surface $\theta_{wb,i,x}$ are plotted in Fig. 4. This figure illustrates the results for three nanoparticle mass concentrations of 0%, 5% and 10%. The influence of the presence or absence of buoyancy effects on the temperature distribution for each case is also investigated. The results are also reported for two Reynolds number of 1000 and 1500.

Fig. 4 shows that at the inlet region, i.e. $x_{bf} < 0$, where the temperature differences are small, the influence of the buoyancy on the non-dimensional temperatures is negligible. However, in the heated sections the buoyancy effect induces a notable change in the temperatures. Indeed, in all cases, the presence of the buoyancy effect reduces the bulk non-dimensional temperature as well as the channel surface temperature. The buoyancy effect induces a secondary circulation flow in cross section of the channel as was observed in Fig. 3. The circulation flow tends to uniformly mix the flow inside the channel and results in a more uniform temperature distribution compared to a fully developed velocity profile. In the case of $Re_{bf} = 1000$, the influence of the buoyancy effects is more obvious compared to that of $Re_{bf} = 1500$. The increase of Reynolds number boosts the convective heat transfer and diminishes the

Table 1
The maximum temperature value and wall temperature drop of the two heating sections for alumina nanofluid with $\omega_{np} = 5\%$ and $\omega_{np} = 10\%$ under different Reynolds numbers.

ω_{np} (%)	Property	Re_{bf}			
		500	1000	1500	2000
5%	$T_{h,1,max}$ °C	79.25	70.61	66.29	63.92
	$T_{h,2,max}$ °C	91.11	80.41	75.09	72.09
	$\varepsilon_{T,h,1,max}$ (%)	1.28	0.35	0.33	0.13
	$\varepsilon_{T,h,2,max}$ (%)	1.15	0.31	0.27	0.19
10%	$T_{h,1,max}$ °C	79.09	70.30	66.15	63.58
	$T_{h,2,max}$ °C	90.92	80.04	74.89	71.66
	$\varepsilon_{T,h,1,max}$ (%)	1.48	0.79	0.54	0.41
	$\varepsilon_{T,h,2,max}$ (%)	1.36	0.77	0.27	0.40

Table 2
The increase of the pressure drop by using nanoparticles for various values of Reynolds number when $q''_{h,1} = q''_{h,2} = 19.4(W/cm^2)$.

Re_{bf}	Pressure drop (Pa)			$\varepsilon_{p\ (\Delta pnf-\Delta pbf\ /\Delta pbf)}$	
	ω_{np} = 0%	ω_{np} = 5%	ω_{np} = 10%	ω_{np} = 5%	ω_{np} = 10%
500	134.2	157	189.1	17.0	41.0
1000	307.5	361.5	427.4	17.6	39.0
1500	484.2	571.2	670.7	18.0	38.5
2000	650.5	782.4	915.3	20.3	40.7

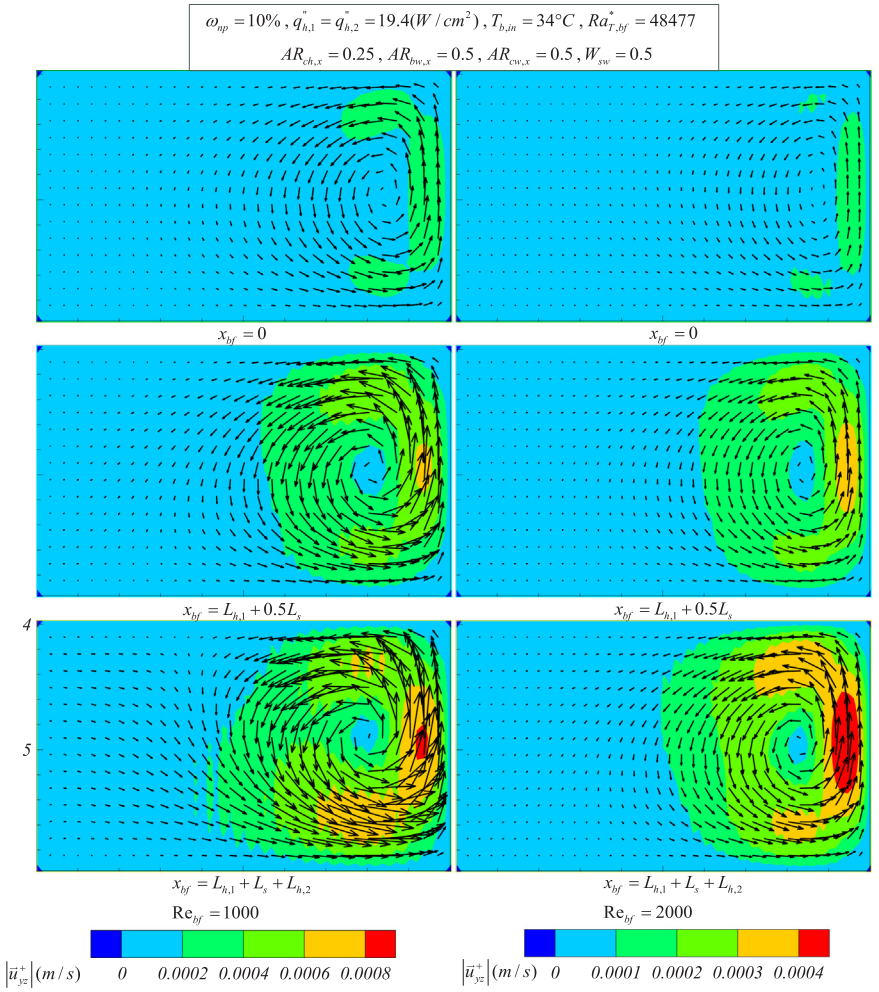

Fig. 3. Velocity contours and vectors of nanofluid in various channel sections in the presence and absence of the buoyancy effects, ω_{np} = 10% and for two cases of Re_{bf} = 1000 and Re_{bf} = 2000.

Table 3
The pressure drop (Pa) in the channel with buoyancy effects for various Reynolds number when $q''_{h,1} = q''_{h,2} = 19.4(W/cm^2)$.

Re_{bf}	Buoyancy is considered			$\varepsilon_{p\ (\Delta pnf-\Delta pbf\ /\Delta pbf)}$	
	ω_{np} = 0%	ω_{np} = 5%	ω_{np} = 10%	ω_{np} = 5%	ω_{np} = 10%
500	106.1	123.9	148.8	16.8	40.3
1000	245	287.2	338.8	17.28	38.3
1500	383.4	451.8	530.1	17.8	38.3
2000	522.8	617.8	722.5	18.2	38.2

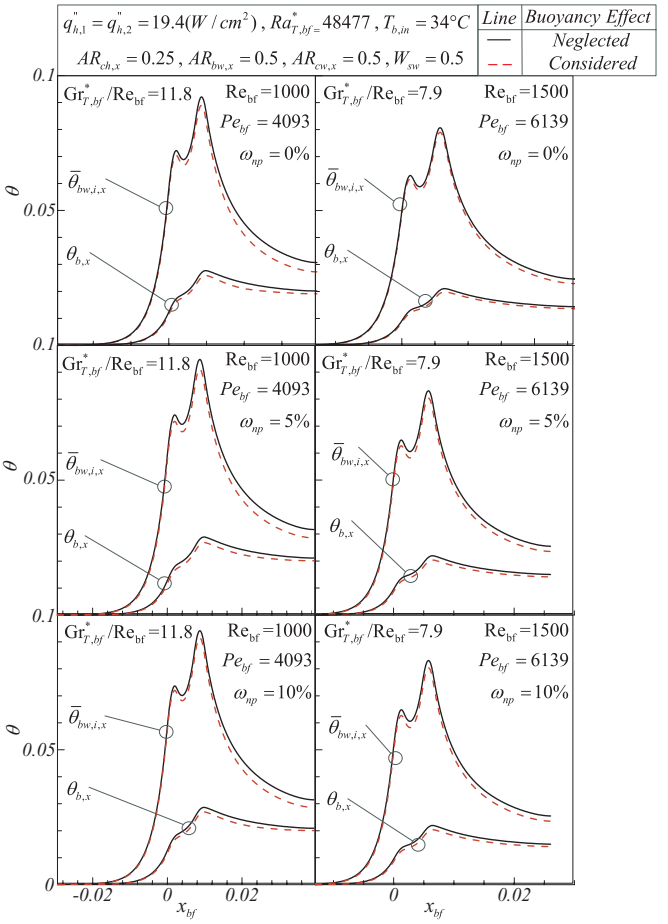

Fig. 4. The effect of heat flux and volume fraction of nanoparticles on the bulk temperature of nanofluid along the flow direction in the presence and absence of buoyancy effects.

effect of secondary flows. The presence of nanoparticles slightly shifts the temperature profiles, but it does not show any effect on the trend of the results.

Fig. 5 compares the temperature ratio of Al_2O_3 water nanofluids in the presence and absence of the buoyancy effects. The results are reported for nanoparticle mass fraction of ω_{np} = 5% and two Reynolds numbers of Re_{bf} = 1000 and Re_{bf} = 2000. This figure shows that the presence of buoyancy effects reduces the nanofluid temperature in the inlet and heating sections. However, in the presence of buoyancy effects, a significant climb in the temperature ratio can be observed toward the outlet. This figure shows that the increase of the Reynolds number diminishes the buoyancy effects.

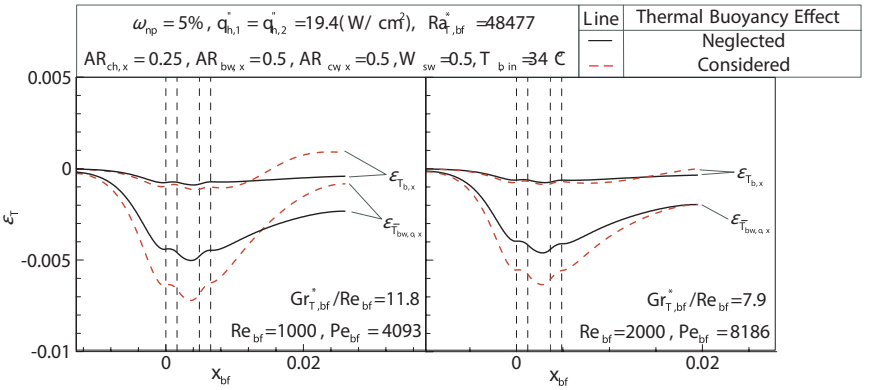

Fig. 5. Temperature ratio of Al_2O_3 water nanofluids and water along the flow direction at different Reynolds numbers with and without the buoyancy effects.

Fig. 6 shows the temperature difference between the bulk temperature of the nanofluid in the channel section and the average temperature of the surface of the bottom wall. The results are reported for two mass fractions of ω_{np} = 5% and ω_{np} = 10% and two Reynolds numbers of Re_{bf} = 1000 and Re_{bf} = 2000. This figure indicates that the presence of buoyancy effects reduces the temperature difference between the bottom wall surface and the bulk temperature of the nanofluid. The trend of behaviour for the two mass fractions of nanoparticles is almost identical. At the adiabatic section of the inlet, the temperature difference is negligible in the presence and absence of buoyancy effects. Next to the heating zones where the buoyancy forces get stronger, the buoyancy effect induces the secondary flows and enhances the heat transfer between the fluid and the channel walls. Hence, the presence of the buoyancy effects reduces the temperature difference between the wall and the fluid. This effect diminishes by the increase of Reynolds number. The increase of Reynolds number boost the primary flow, and hence, reduces the effect of secondary buoyancy flows.

5. Conclusion

The heat transfer of Al_2O_3 water nanofluid in a mini-channel with highly thermal conductive thick walls is theoretically studied. There are two discrete heat sources with constant heat flux at the bottom of the channel. The governing equations for fluid continuity, momentum and heat transfer in the nanofluid and heat transfer in the channel walls are introduced in three dimensional space and transformed in non-dimensional form using non-dimensional parameters. The finite volume method is employed to solve the governing equations. The results are compared with some cases in the literature and good agreement were found. The effect of various concentrations of nanoparticles on the heat transfer of the channel is studied. The effect of Reynolds number and heat flux intensity on the thermal behaviour of mini-channel is investigated. The influence of the buoyancy effects on the channel heat transfer is also addressed. The results are reported in the form of contours, bulk temperature, plots of heat transfer enhancement and tables. The pressure drop for the nanofluid in the presence and absence of buoyancy effects is evaluated and reported. The main outcomes of the present study can be summarized as follows:

1. It is found that the axial heat transfer in millimeter size channels is important and cannot be neglected. This outcome holds true for low and high values of Reynolds number.
2. By moving in the flow direction from the inlet toward the outlet, the bulk temperature of the fluid first increases and then decreases. The increase of the temperature of the nanofluid begins before reaching of the heated zones due to the axial heat transfer mechanisms. When the nanofluid passes over the heated zones, its temperature gradually increases until it reaches the maximum temperature about the end of second heated zone. After that, the temperature reduces again due to the axial heat transfer effects.
3. The increase of the nanoparticles mass fraction reduces the bulk temperature difference in the inlet adiabatic zone and the heated

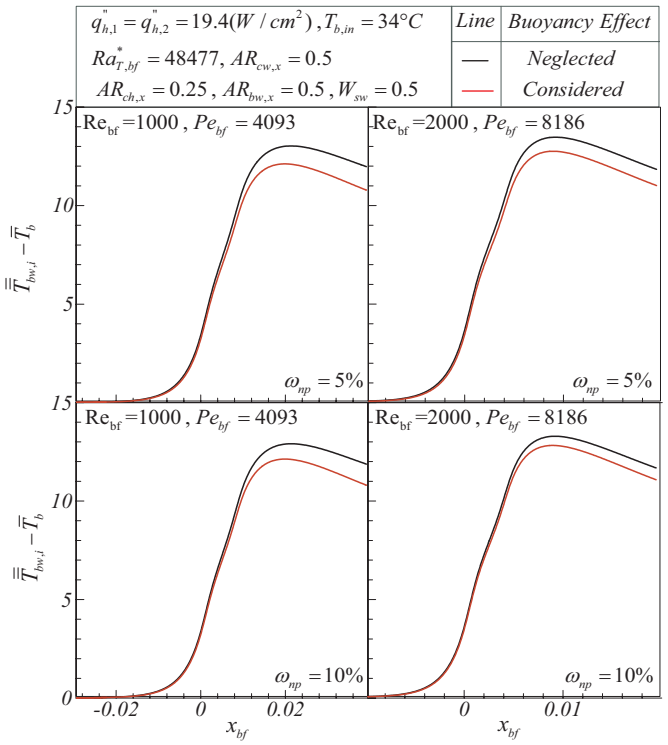

Fig. 6. Temperature difference between the bulk temperature of the fluid and channel wall with/without buoyancy effect in the flow direction.

zones.

4. The buoyancy effect induces a secondary circulation flow in the cross section plane of the min-channel which enhances the heat transfer and reduces the pressure drop in the channel.
5. Although the presence of Al_2O_3 nanoparticles enhances the heat transfer, they also increase the pressure drop which is not of interest. For example, at $Re_{bf} = 500$ and $\omega_{np} = 5\%$, 17% relative pressure drop were observed.

Acknowledgements

The authors appreciates the financial support from Ministry of Science and Technology, Taiwan, under grant number MOST 106–2221-E-027–103. The authors also appreciate the financially supported by the “Research Center of Energy Conservation for New Generation of Residential, Commercial, and Industrial Sectors” from The Featured Areas Research Center Program within the framework of the Higher Education Sprout Project by the Ministry of Education (MOE) in Taiwan.

References

[1] C.J. Ho, P.C. Chang, W.M. Yan, M. Amani, Comparative study on thermal performance of MEPCM suspensions in parallel and divergent minichannel heat sinks, Int. Commun. Heat Mass Transf. 94 (2018) 96–105.
[2] C.J. Ho, C.J. Chang, P.C. Yan, W.M., P. Amani, Efficacy of divergent minichannels on cooling performance of heat sinks with water-based MEPCM suspensions, Int. J. Therm. Sci. 130 (2018) 333–346.
[3] D.B. Tuckerman, R. Pease, High-performance heat sinking for VLSI, Electron Device Lett. IEEE 2 (1981) 126–129.
[4] W. Qu, I. Mudawar, Analysis of three-dimensional heat transfer in micro-channel heat sinks, Int. J. Heat Mass Transf. 45 (2002) 3973–3985.
[5] P.S. Lee, S.V. Garimella, D. Liu, Investigation of heat transfer in rectangular micro-channels, Int. J. Heat Mass Transf. 48 (2005) 1688–1704.
[6] P.S. Lee, S.V. Garimella, Thermally developing flow and heat transfer in rectangular micro-channels of different aspect ratios, Int. J. Heat Mass Transf. 49 (17–18) (2006) 3060–3067.
[7] S. Choi, Enhancing Thermal Conductivity of Fluids with Nanoparticles, ASME-Publications-Fed., 1995, pp. 99–106.
[8] R. Saidur, K.Y. Leong, H. Mohammad, A review on applications and challenges of nanofluids, Renew. Sustain. Energy Rev. 15 (2011) 1646–1668.
[9] K. Khanafer, K. Vafai, A critical synthesis of thermophysical characteristics of nanofluids, Int. J. Heat Mass Transf. 54 (2011) 4410–4428.
[10] K. Khanafer, K. Vafai, A review on the applications of nanofluids in solar energy field, Renew. Energy 123 (2018) 398–406.
[11] O. Mahian, A. Kianifar, S.A. Kalogirou, I. Pop, S. Wongwises, A review of the applications of nanofluids in solar energy, Int. J. Heat Mass Transf. 57 (2) (2013) 582–594.
[12] D.K. Devendiran, V.A. Amirtham, A review on preparation, characterization, properties and applications of nanofluids, Renew. Sustain. Energy Rev. 60 (2016) 21–40.
[13] A. Zaraki, M. Ghalambaz, A.J. Chamkha, M. Ghalambaz, D. De Rossi, Theoretical analysis of natural convection boundary layer heat and mass transfer of nanofluids: effects of size, shape and type of nanoparticles, type of base fluid and working temperature, Adv. Powder Technol. 26 (2015) 935–946.
[14] J. Lee, I. Mudawar, Assessment of the effectiveness of nanofluids for single-phase and two-phase heat transfer in micro-channels, Int. J. Heat Mass Transf. 50 (2017) 452–463.
[15] L. Chuan, X.D. Wang, T.H. Wang, W.M. Yan, Fluid flow and heat transfer in micro-channel heat sink based on porous fin design concept, Int. Commun. Heat Mass Transf. 65 (2015) 52–57.
[16] C. Leng, X.D. Wang, W.M. Yan, T.H. Wang, Heat transfer enhancement of micro-channel heat sink using transcritical carbon dioxide as the coolant, Energy Convers. Manag. 110 (2016) 154–164.
[17] O. Mahian, A. Kianifar, A.Z. Sahin, S. Wongwises, Performance analysis of a minichannel-based solar collector using different nanofluids, Energy Convers. Manag. 88 (2014) 129–138.
[18] C.J. Ho, C.Y. Chang, W.M. Yan, P. Amani, A combined numerical and experimental study on the forced convection of Al_2O_3-water nanofluid in a circular tube, In. J. Heat Mass Transf. 120 (2018) 66–75.
[19] C.J. Ho, W.C. Chen, W.M. Yan, M. Amani, Cooling performance of MEPCM suspensions for heat dissipation intensification in a minichannel heat sink, Int. J. Heat Mass Transf. 115 (2018) 43–49.
[20] I.A. Ghani, N.A.C. Sidik, N. Kamaruzzaman, W.J. Yahya, O. Mahian, The effect of manifold zone parameters on hydrothermal performance of micro-channel heatsink: a review, Int. J. Heat Mass Transf. 109 (2017) 1143–1161.